Desalination and Water Treatment
www.deswater.com
doi: 10.5004/dwt.2020.25100

181 (2020) 27–39
March

Nanofiltration performance prediction for brackish water desalination: case study of Tunisian groundwater

Mohamed Ayman Kammoun[a,b], Sana Gassara[b], John Palmeri[c], Raja Ben Amar[a], André Deratani[b,*]

[a]*Laboratoire Sciences des Matériaux et Environnement, Université de Sfax, Faculté des Sciences de Sfax, Rte. De Soukra Km 4, Sfax, Tunisia, emails: mohamadaymankamoun@gmail.com (M.A. Kammoun), benamar.raja@yahoo.com (R.B. Amar)*
[b]*Institut Européen des Membranes, IEM, UMR-5635, ENSCM, CNRS, Univ Montpellier, Montpellier, France, emails: gassarasana@yahoo.fr (S. Gassara), andre.deratani@umontpellier.fr (A. Deratani)*
[c]*Laboratoire Charles Coulomb (L2C), Univ Montpellier, CNRS, Montpellier, France, email: john.palmeri@umontpellier.fr (J. Palmeri)*

Received 9 July 2019; Accepted 26 October 2019

ABSTRACT

In response to the fresh water scarcity, Tunisia is utilizing more and more membrane desalination of unconventional resources, including brackish waters and seawater. The widespread reserves of groundwaters and their low salinity make this resource of special interest. Two predominant ionic compositions have been identified depending on their relative proportion of sulfate to chloride ions. The question arising for the decision-makers concerns the choice of membrane technology and, therefore, of membrane. Two nanofiltration (NF) membranes (NF270 and NF90) and a reverse osmosis (RO) one (BW30) were tested in a desalination study of synthetic feeds reproducing the ionic composition of three representative groundwaters. Sulfate/chloride ratio appears to be the key factor for the membrane choice to obtain good quality drinking water meeting the Tunisian standards. Moreover, validation of two prediction tools was investigated: ROSA, software provided by the membrane manufacturer and Nanoflux®, software specifically designed for NF. The experimental NF results are well fitted by the Nanoflux® simulations. We concluded that ROSA cannot generally provide good NF predictions because it does not take into account the electric interactions between membrane and feed.

Keywords: Membrane desalination; Groundwater; Nanofiltration; Performance prediction; Software validation

1. Introduction

The Southern Mediterranean countries have been identified as undergoing one of the most important water crises in the world. This is the case for Tunisia, one of these countries, which has been suffering for several years from a water shortage that makes problematic the drinking water supply in some areas and at particular times of the year. Several studies predict that rising living standards and the development of the agriculture, industry and tourism sectors will exacerbate the water scarcity in such a way that supply disruption could be extended to the whole of the country [1]. Indeed, according to the Tunisian national water supply agency (SONEDE), the consumption of drinking water, which attained 381 Mm^3 in 2010, is expected to increase to 450 and 500 Mm^3 in 2020 and 2030, respectively [2].

Considering the growing water scarcity and the increasing demand for drinking water, Tunisia is moving more and

* Corresponding author.

more towards the exploitation of unconventional resources including brackish groundwater reserves and, more recently, seawater. Tunisian groundwaters can be roughly classified into two predominant types of brackish waters: (i) those coming from deep aquifers with a salinity between 1.5 and 3 g L^{-1} comprising a high proportion of sulfate, calcium and magnesium divalent ions (type 1) and (ii) those coming from sedimentary coastal aquifers with a salinity between 3 and 5 g L^{-1} (type 2) [3]. In recent years, the salinization of the latter has resulted from intrusion of marine water caused by the over-exploitation of these resources. In this case, the main contaminants are the chloride and sodium ions [4].

Desalination becomes then essential to avoid soil sterilization in agricultural watering and to make water suitable for human consumption and everyday household needs [5]. Reverse osmosis (RO) is the most common membrane technology used for performing this task [6]. This process, based on dense membranes operating at high pressure, produces overqualified permeate in most of the cases [7]. Therefore, RO suffers from the following three key limitations: high energy consumption, low water recovery, and excessive membrane fouling [8–10]. Nowadays, for obvious economic reasons, one the most important issues is the energetic impact of the RO desalination process. One way of overcoming this challenge is the integration of technologies less demanding in terms of energy consumption, such as nanofiltration (NF). NF shows clear advantages over RO, including higher permeate fluxes and lower operating pressure, resulting in lower investment costs. Moreover, although ion rejection is lower than for RO technology, requirement specifications can often be met using NF, thereby providing a better cost-effective option in many cases [11–14].

In contrast to RO, NF membranes are considered as porous and exhibit nominal cutoffs between 200 and 1,000 Da [11,15]. Only the membranes with the tightest pores are used for desalination treatment. Two groups can be distinguished in the literature regarding the rejection of monovalent ions (NaCl), as non-exhaustively presented in Table 1.

The first group, including, for example, the NF270 (Dow Filmtec, USA), NFX (Synder, USA), DK (GE osmonics, USA) NF membranes, is characterized by a high selectivity between monovalent and divalent ions for single solutions with typical rejections of less than 60% (NaCl) and higher than 90% ($MgSO_4$), respectively. On the other hand, these membranes offer higher permeate flow rates than the second group (Table 1), which have rejection properties closer to RO membranes. The 1st membrane group is generally suggested for cutting down the total hardness of surface, sea and groundwaters due to their high mono/divalent ion selectivity [22–24] while the 2nd group is preferred for removing the total salinity and pollutants [25]. However, it was also reported that the NaCl concentration has a strong impact on salinity removal performance.

Therefore, the data in Table 1 are only indicative as the ion composition of real solutions and the precise plant configuration and operating conditions all have a dramatic effect on the performances of NF membranes. The electrostatic interactions between the ionic species in a multi-component feed and between the ions and the membrane charge are highly non-linear and cannot, in general, be predicted straightforwardly using as sole input single salt rejections performances. There are furthermore currently ill-understood non-electrostatic interactions (steric, dielectric, hydration) that complicate quantitative modeling [26]. It is, therefore, usually impossible to predict the NF performance of a given membrane and therefore judge its suitability for a given application from the limited performance characteristics communicated by the membrane manufacturers.

The question that arises from the previous discussion is how to decide which kind of membrane technology (NF or RO) and membrane should be used for desalting the different types of Tunisian groundwaters. This requires having an efficient modeling tool to save time by limiting the number of experimental validations. In the case of RO, most of the manufacturers provide prediction software such as, for example, ROSA (Dow Filmtec, USA) [27]. For the reasons mentioned above, it is more difficult to have the equivalent for NF. It should be noted that the ROSA software, which is well-recognized as a suitable tool for estimating RO membrane performance in relation to the plant operating conditions, also has an NF database. In this paper, comparison of performance prediction with the Nanoflux® software, which is well adapted for NF transport mechanism, was carried out in the case of the NF270 and NF90 membranes, each being associated with a different group (Table 1). To do so, we confronted the model predictions with the results of filtration experiments carried out using the two simulated major types of Tunisian groundwaters. The obtained data were discussed in terms of water quality and productivity efficiency in order to optimize the membrane and process choice vs. the ground water ionic composition.

Table 1
Some commercial nanofiltration membranes classified with respect to their mono- and divalent salt rejection

	Membrane	Manufacturer	NaCl rejection (%)	$MgSO_4$ rejection (%)	Reference
1st Group	NF270	Dow Filmtec, USA	50	>98	[16]
	NFX	Snyder, USA	40	99	[17]
	Trisep TS40	Microdyn Nadir, Germany	40	99	[18]
	DK, DL	GE Osmonics, USA	<50	>98	[11,19]
2nd Group	NF90	Dow Filmtec, USA	>90	>98	[16]
	Trisep TS80	Microdyn Nadir, Germany	80	99	[20]
	ESNA1	Nitto Hydranautics, Japan	>80	>86 ($CaCl_2$)	[21]

2. Materials and methods

2.1. Theory

The structure of NF membranes was assumed to be a bundle of straight cylindrical capillaries characterized by their pore radius r_p and effective length l_{eff} (Fig. 1) and the external solutions to be ideal and perfectly stirred so that concentration polarization could be neglected in the present study. The system was considered isothermal with a temperature T of 298 K. The composition of the feed was fixed by the concentration of the N ions making up the mixture, each denoted by a concentration C_i^f (i = 1…N). In the same way, C_i^p and $\bar{c}_i$ denote their concentration in the permeate and inside the membrane, respectively.

The solute rejection in NF is described as being the result of the following steps: a distribution of charged species at the membrane – solution interface caused by the steric and electrostatic exclusion mechanisms and a transfer by a combination of convection, diffusion and electric migration through the membrane. The NF transfer is generally described using the hindered electro-transport (HET) model that is based on the volume averaged Stokes equation for solution flow and incorporates steric and hydrodynamic hindrance factors into the Extended Nernst Planck (ENP) ion flux equations and steric/Donnan partitioning at the membrane/solution interfaces [28–30].

$$j_i = -K_{i,d}\overline{D}_i\frac{d\bar{c}_i}{dx} - \frac{z_i\bar{c}_iK_{i,d}\overline{D}_i}{RT}F\frac{d\phi}{dx} + K_{i,c}\bar{c}_iJ_v \tag{1}$$

with $\overline{D}_i = D_i\, l_m / l_{\text{eff}}$ the effective diffusion coefficient of ion i in the membrane, $K_{i,d}$ the diffusive hindrance factor for ion i, D_i the bulk diffusion coefficient of ion i, $\bar{c}_i(x)$ the concentration of ion i in the membrane, z_i the ion valance, R the gas constant, T the temperature, F the Faraday constant, ϕ the electric potential in the membrane, $K_{i,c}$ the convective ion hindrance factor (J_v is the volume flux density based on the membrane area). Eq. (1) has to be coupled with an explicit expression of the local electroneutrality inside pores:

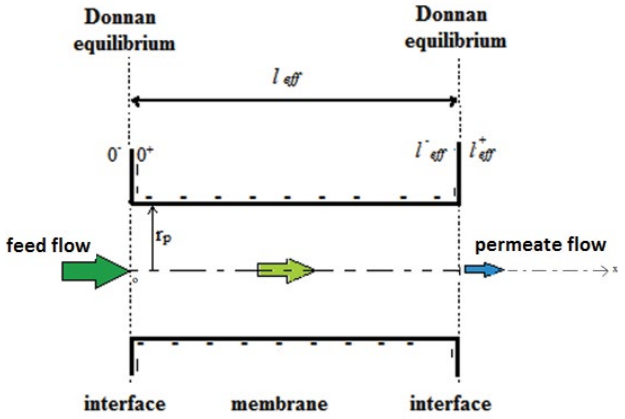

Fig. 1. Schematic diagram of a membrane pore used in the modeling with r_p the pore radius and l_{eff} the effective pore length. The positions 0^- and l_{eff}^+ denote the axial coordinates just outside the pore, 0^+ and l_{eff}^- denote the axial coordinates just inside the pore.

$$\sum_{i=1}^{N} z_i\bar{c}_i + X_m = 0 \tag{2}$$

where $X_m = \dfrac{2\sigma}{Fr_p}$ is the effective membrane charge (moles/m^3 of pore volume) for cylindrical pores and related to the surface charge density σ. The normalized membrane charge X_i is defined as:

$$X_i = \frac{X_m}{C_{\text{tot}}} \tag{3}$$

with C_{tot} is the total salt concentration. Furthermore, in NF, the electric current density across the membrane vanishes

$$J_c = F\sum_{i=1}^{N} z_iJ_i = 0 \tag{4}$$

which allows one to obtain a relation between the electric potential gradient and the ionic concentrations. The volume averaged Stokes equation is given:

$$\frac{1}{L_p^0}J_v = -\frac{dP}{dx} - \rho\frac{d\phi}{dx} \tag{5}$$

where L_p^0 is the pure water permeability and $\rho = F\sum_{i=1}^{N} z_i\bar{c}_i$ the local ion charge density.

In NF, the HET equations must be solved using the filtration condition boundary. First, the ionic molar fluxes J_i are related to solution volume flux J_v as follows:

$$J_i = C_i^pJ_v \tag{6}$$

Second, the distribution of ions at the membrane/solution interfaces is described by the following modified Donnan equations:

$$\bar{c}_i(0^+) = C_i^f\Phi_i\exp\left[\frac{-z_i\,F\Delta\phi_{D(0^-|0^+)}}{(RT)}\right] \tag{7}$$

$$\bar{c}_i(l_{\text{eff}}^-) = C_i^p\Phi_i\exp\left[\frac{-z_i\,F\Delta\phi_{D(l_{\text{eff}}^+|l_{\text{eff}}^-)}}{(RT)}\right] \tag{8}$$

where $0^-|0^+$ and $l_{\text{eff}}^-|l_{\text{eff}}^+$ denote the membrane/solution interfaces at the feed side and the permeate side, respectively. Φ_i is the steric partitioning coefficient of ion i defined as the ratio between the available section (i.e., taking into account the finite size of the ion) and the pore cross section and $\Delta\phi_D$ is the dimensionless Donnan potential arising at each nanopore/external solution interface.

Finally, at the one membrane element level theoretical ion rejection predictions for multi-electrolyte solutions can be obtained from the following equation:

$$R_i = 1 - \frac{C_i^p}{C_i^f} \tag{9}$$

NanoFlux® is a commercial nanofiltration simulation program (CNRS) that can solve numerically the HET model for up to 11 ionic species and composite membrane systems with up to three distinct layers. Given the composition of the feed solution, the characteristics of the membrane, and the configuration of the NF installations, NanoFlux® uses an internal single salt database to predict the NF performance for arbitrary ionic mixtures in terms of ionic rejection and volume flux density [31–34].

2.2. Experimental part

2.2.1. Materials

Two commercial NF membranes (NF90 and NF270) and one RO membrane (BW30) from Dow Filmtec (USA) were used in this work. The solutions used to characterize the charge and the performance properties of the membranes were prepared by dissolving salts of analytical grade salts without further purification in deionized water (18 MΩ/cm, Millipore Milli-Q): NaCl, $CaCl_2$, Na_2SO (Carlo Erba) and $MgSO_4$ (Merck Eurolab). All the solutions were filtered (0.45 μm) prior to use to remove the residual insoluble impurities.

2.2.2. Nanofiltration pilot

Tangential filtration experiments were carried out using a nanofiltration pilot (Fig. 2) consisting of a feed tank (1) equipped with a temperature control loop (2), a positive displacement pump (3), a 2.5″ stainless steel pressure vessel accommodating 2,540 filtration elements (4), a pressure regulating valve (5) and a sampling loop (6). A programmable logic controller (7) is used to control the equipment and to retrieve the data from the sensors (feed and permeate flow, feed pressure and retentate, feed tank level). Sampling loop sensors allow pH, temperature and conductivity measurements of the retentate and permeate. The flow rate of the feed was set at 7.9 L min^{-1}. The membranes were first immersed at least overnight in water before being used in any experimental work and each membrane was conditioned by filtering pure water at 17 bar during 1 h to avoid any compression effects and to establish leak tightness. All filtration experiments were carried out with an applied pressure range of 2–15 bar at room temperature (25°C).

Fig. 2. Presentation of the nanofiltration pilot used in this study: (1) feed tank; (2) temperature control loop; (3) pressure pump; (4) 2.5″ stainless steel pressure vessel; (5) pressure regulating valve; (6) sampling loop; (7) programmable logic controller.

2.2.3. Permeability measurement

Membrane permeability was determined from the volume flux (J_v) by circulating water through the membrane system. J_v (L m^{-2} h^{-1}) was calculated using Eq. (10):

$$J_v = \frac{V_p}{(\Delta t \times A)} \tag{10}$$

where V_p (L) is the volume of permeate, Δt (h) is the permeation time and A (m^2) is the active membrane surface area. Membrane permeability (L m^{-2} h^{-1} bar) was determined from the slope of the linear variation of J_v as a function of applied pressure P (bar).

2.2.4. Ionic composition of simulated brackish waters from South Tunisia

The major ion composition is reported in Table 2 for groundwater found in three locations of South Tunisia that were selected as a function of their sulfate/chloride ratio and salinity. Sfax well 1 is representative of type 1 brackish waters (sulfate/chloride ratio > 1 and salinity < 3 g/L) and Sfax well 2 and Gabés of type 2 ones (sulfate/chloride ratio < 1 and salinity > 3 g/L). Synthetic waters were prepared from the compositions reported in Table 2 and denoted Feed 1, Feed 2 and Feed 3, respectively. Each of these parameters is compared with the corresponding value of Tunisian standards for drinking water. The ion composition did not show the presence of HCO^{-3} at least not to a large extent. Feed 3 contains about 188 mg/L accounting for the higher pH value of 8. This concentration is, however, low compared with the other ones and was, therefore, not considered a relevant parameter even if it was taken into account in the preparation of the simulated feed.

2.2.5. Salt rejection measurement

The salt concentrations in permeate and feed solutions were determined by ion chromatography (DIONEX ICS-1000, USA) analysis. The salt rejection was calculated using Eq. (9).

2.2.6. Zeta potential

The zeta potential is the electric potential in the interfacial double layer at the location of the slip plane relative

to a point in the bulk fluid away from the interface. It characterizes the membrane surface charge and can be used for the quantification of its magnitude. The membrane surface zeta potential was determined with a SurPASS electro-kinetic analyzer (Anton Paar, GmbH, Austria) based on the streaming potential method. An adjustable gap cell in which the membrane samples were mounted was used with a height of about 100 μm [35,36]. The KCl electrolyte solution at different concentrations was circulated in the cell between two pieces of membrane that were immersed in the electrolyte overnight before the measurement. The pH of the electrolyte was controlled by HCl 10^{-1} M and NaOH 10^{-1} M solutions. The zeta potential was calculated using the Helmholtz–Smoluchowski equation from the measured streaming voltage as a function of pH (from pH 4 to pH 10).

3. Results and discussion

Three simulated solutions with ionic compositions representative of brackish groundwaters found in South Tunisia (Table 2) were filtered using two NF membranes (NF90 and NF270) and one RO membrane (BW30) for comparison. The salinity spans the range of 2,222–5,394 mg/L with sulfate/chloride ratio varying from 2 to about 0.5. Two different NF modeling tools (Rosa and Nanoflux® available from Dow Filmtec, USA and CNRS, respectively) were used to predict the permeate flow rate and the salt rejection as a function of the applied pressure in the range of 2–14 bar. The obtained simulation results were compared with the experimental ion rejection data.

3.1. Desalination performances of NF and RO membranes

Feed 1 is characterized by the lowest salinity with a value that exceeds the standard of Tunisian regulation for drinking water (Table 2) by only 10%. However, it contains high concentrations of sodium and sulfate ions with values that exceed the norms by 65% and 50%, respectively. Feed 2 has intermediate salinity (3,337 mg/L) with high concentrations of sodium, chloride and sulfate exceeding the standards by approximately 76%, 64% and 37%, respectively. Considering these data, it was expected that NF could lead to permeate with composition meeting the Tunisian regulation for drinking water. Fig. 3 shows the NF90 and NF270 performances in terms of filtration flux (J_v) and permeate salinity as a function of the applied pressure for Feed 1 and Feed 2.

The membrane permeability values obtained from the linear variation of J_v as a function of the applied pressure are seen to be decreasing with increasing feed salinity (from Feed 1 to Feed 2, Table 3). The intensity of this effect, however, is strongly dependent on the rejection rate, as it is more than four times higher in the case of the NF90 membrane (group 2). This observation can be accounted for by an apparent viscosity enhancement in nano-scale pores (electroviscous effect) related to electrostatic interactions between the membrane charges, the ions in solution and water: the flow induced streaming potential acts back on the ions in solution to reduce the flow driving force produced by the transmembrane pressure gradient, leading to a decrease in slope that can be interpreted as an enhanced apparent viscous (on the other hand at the relatively low salt concentrations studied osmotic pressure effects are weak) [30,32].

As expected from the diffusion/convection transfer mechanism, the passage of ions across the membrane decreases with an increase of applied pressure (Fig. 3). At low pressure and permeate flow rate, the weak concentration difference between both sides of the membrane induced by the convective transport is counterbalanced by diffusive transport from the concentrated solution to the diluted one which enables a high passage of ions. The permeate flux increases with the trans-membrane pressure reducing the diffusion contribution with respect to convection leading to the observed decrease of ion passage until a high-pressure plateau is reached.

Feed 2 mainly differs from Feed 1 by its chloride content, which is about three times higher (Table 2). The lower rejection of monovalent ions by membranes of group 1 could then primarily be responsible for the strong decrease of ion rejection from Feed 1 to Feed 2 observed in the case of the NF270 membrane (Table 3). Another important factor is related to how an increase of salinity in the feed solution causes the screening of membrane charges, thereby inducing a reduction of Donnan exclusion and resulting in an alteration of both NF membrane performances. It should

Table 2
Physicochemical parameters of three brackish groundwaters found in the south of Tunisia compared with the Tunisian standards for drinking water

Parameters	Sfax well 1 (Feed 1)	Sfax well 2 (Feed 2)	Gabés (Feed 3)	Tunisian standards NT 09.14 (2013) [5]
pH	6.2	6	8	6.5–8.5
Na^+ (mg/L)	571	837	1,430	200
Cl^- (mg/L)	500	1,400	1,900	500
Mg^{2+} (mg/L)	77	99	106	100
Ca^{2+} (mg/L)	74	208	320	200
SO_4^{2-} (mg/L)	1,000	793	1,450	500
HCO_3^- (mg/L)	–	–	188	–
Salinity of simulated solutions (mg/L)	2,222	3,337	5,394	200–2,000

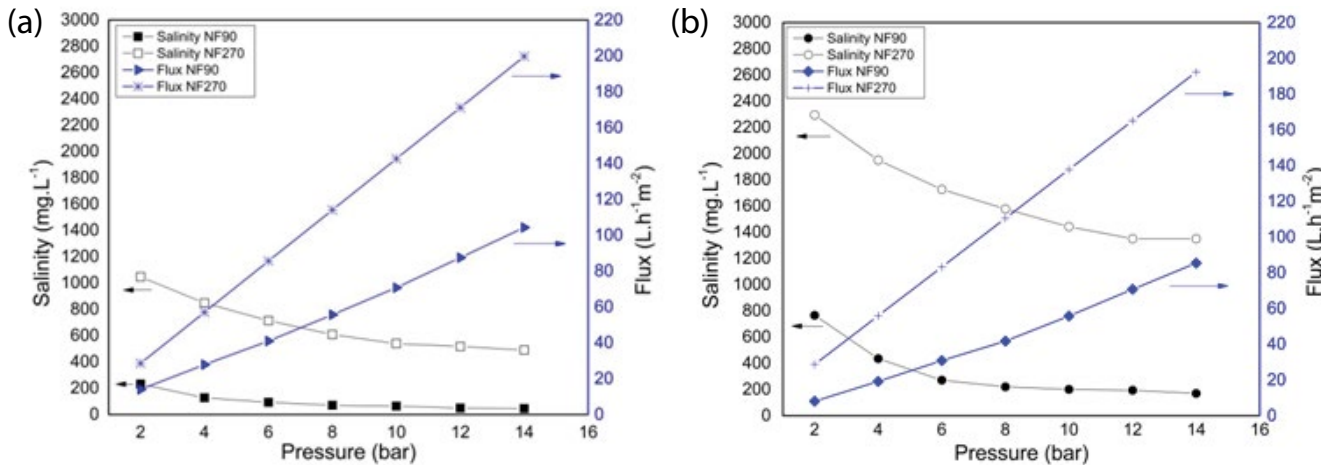

Fig. 3. Effect of pressure on permeate flux and salinity for filtration of Feed 1 (a) and Feed 2 (b) using the NF90 and NF270 membranes.

Table 3
Membrane permeability and salinity rejection at 10 bar for filtration of Feed 1and Feed 2 using the NF90 and NF270 membranes

Membrane	Feed 1		Feed 2		Feed 1/Feed 2	
	Permeability ($L.m^{-2}\ h^{-1}$ bar)	$R^{10\ bar}_{salinity}$ %	Permeability ($L.m^{-2}\ h^{-1}$ bar)	$R^{10\ bar}_{salinity}$ %	Permeability decrease%	Rejection decrease %
NF270	14.3	75.7	13.7	55.3	4	29
NF90	7.4	97.1	6.2	93.8	17	4

be noted that the water quality produced in all cases is in accordance with the Tunisian standards in term of salinity (<2,000 mg/L). However, treatment of Feed 1 by NF90 leads to permeate with a too low-level salinity requiring a remineralization operation. The ion composition of permeates obtained using NF270 and NF90 membranes at respective transmembrane pressure of 6 and 10 bar (recovery about 15 %) is given in Table 4. The value of 10 and 6 bar was chosen since it appears to be a good compromise between salinity removal and applied pressure. In that case, most permeates fully comply with the Tunisian standards for drinking water as defined in Table 2 except in the case of treatment of Feed 2 by NF270 where the sodium and chloride contents in the permeate exceeded the required values. These results confirm that membranes of group 1 are not appropriate for treating waters with too high content in monovalent ions due to their high divalent/monovalent selectivity.

To continue the comparison, NF270 is more productive and less energy consuming in terms of filtration flux than NF90 whereas its permeate salinity is much higher. NF270 (and group 1 NF membranes) can be considered as the right choice to treat Tunisian groundwaters with a low NaCl content without any need to remineralize permeate. On the other hand, NF90 (and group 2 NF membranes) are particularly well-suited to treat waters similar to Feed 2.

To highlight in greater detail the behavior of the two studied membranes, representative of the two groups defined in introduction (Table 1), the rejection performance for each ion is reported in Fig. 4.

The difference in separation performance between the two membranes is related to their porous structure, as NF270 is known to have a larger pore size than that of NF90 [37,38]. Moreover, they both have a negatively charged surface at neutral pH as determined by their zeta potential [38]. Owing to its restricted pore size, which impedes the convective and diffusive mobility of ions, NF90 can retain more than 98% of the divalent ions and about 90 % of the monovalent ones for the two types of feed solutions. The quasi-quantitative rejection of sulfate ions by the two membranes originates from strong electrostatic interactions between the –2 ion charge and the membrane surface. In contrast to NF90, NF270 rejects more selectively divalent anion than divalent cations. Actually, cations act as membrane counter-ions and their passage depends on the rejection of the other ions to ensure the electroneutrality of concentrate and permeate according to the Donnan equilibrium effects. In the case of Feed 1, the sulfate feed concentration is higher than that of chloride. The divalent Mg^{2+} and Ca^{2+} cations are, therefore, highly retained to ensure electroneutrality in the concentrate. By contrast, in the case of Feed 2, the chloride feed concentration is higher than that of sulfates. The passage of chloride through the membrane because of its lower valance, smaller size and its high mobility causes the passage of a certain number of divalent counter ions (besides the monovalent ones) to ensure electroneutrality in both permeate and concentrate sides. Consequently, the rejection of divalent cations is greater in the case of Feed 1 than in Feed 2 [37]. In all cases, chloride can be seen in Fig. 4 as the less retained ion and appears to be a discriminating and limiting parameter. Then, monitoring the concentration of chlorides in permeate is essential to verify the compliance of nanofiltered water with the standards.

Table 4:
Ion composition of permeates and productivity at 6 bar (NF270) and 10 bar (NF90)

		SO_4^{2-} mg/L	Cl^- mg/L	Mg^{2+} mg/L	Ca^{2+} mg/L	Na^+ mg/L	Salinity mg/L	Permeate flow rate L/h m^{-2}	Recovery (%)
NF270	Feed 1	55.4	384	9	11.2	245.7	705.3	85.6	18
	Feed 2	24.8	1,207[a]	15.2	46.8	433[a]	1,727	83.2	17.5
NF90	Feed 1	5.7	37	0.58	0.67	21	65[a]	71	15.6
	Feed 2	2.9	137	0.52	2.4	59	201	56	13.1

[a]Not complying with the Tunisian standards for drinking water.

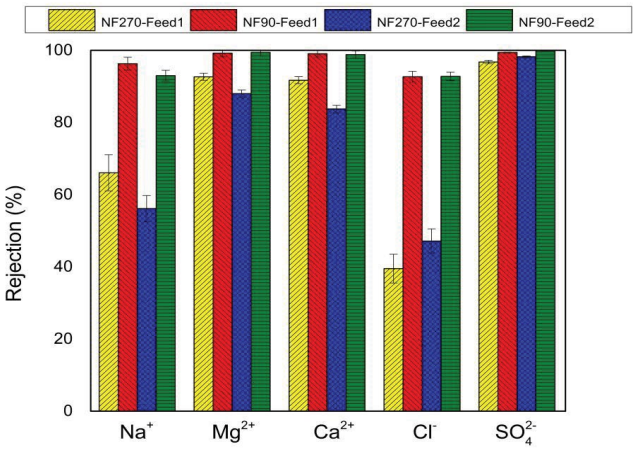

Fig. 4. Rejection of monovalent and bivalent ions by NF270 and NF90 membranes at a fixed trans-membrane pressure of 10 bar for Feed 1 and Feed 2.

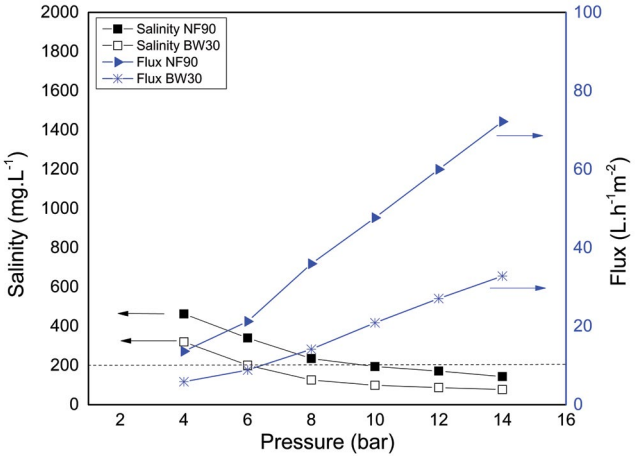

Fig. 5. Effect of pressure on permeate flux and salinity for filtration of Feed 3 using the NF90 and BW30 membranes. The dashed line represents the lower limit of Tunisian salinity norm.

To conclude this part, it is really interesting to compare the performance of brackish water reverse osmosis (BWRO) membranes with that of the group 2 NF ones. Fig. 5 shows the variation of permeate flow rate and salinity as a function of applied pressure for filtration using NF90 and BW30 in the case of the groundwater Feed 3 having a higher salinity than Feed 1 and Feed 2 with a large content of both chloride and sulfate anions. The salinity of permeate meets the requirement of Tunisian standards for optimum applied pressures of about 10 and 6 bar in the case of NF90 and BW30, respectively. Beyond these values, the permeate needs to be remineralized. It should be noted that all the ion parameters are fully in compliance with the requirement of the Tunisian regulation for drinking water. Table 5 shows the parameters of permeates obtained with the two membranes at applied pressures of 10 and 14 bar. These data are given only for comparison as the recovery rates are too low for an efficient BW30 operation. Again, NF appears to be the better solution for the production of drinking water from this type of groundwater both in terms of productivity and desalination performance.

At this point, it is obviously essential to have a prediction tool to decide what kind of membranes (NF group 1 and 2 membranes or BWRO) could be best suited in terms of desalination performance and specific energy consumption estimated by the produced volume of desalinated water at a given pressure depending on the feed groundwater salinity and ionic composition (sulfate and chloride anion content). This is the objective of the following section in which two available softwares (ROSA and Nanoflux®) were tested and their simulation data confronted with the previous experimental results.

3.2. Nanofiltration performance prediction: software validation

3.2.1. ROSA prediction

As above mentioned, ROSA is popular software and well-established prediction tool used successfully for the performance assessment and design of RO systems [27]. This is illustrated by the modeling of ion rejections obtained in the case of Feed 3 treated with the BWRO membrane BW30. Although comparison with the experimental data in Fig. 6 shows only fairly good overall agreement for all the ions studied, in the domain close to the rejection plateau (applied pressure beyond 10 bar) the agreement is excellent with deviations of less than 1%.

The ROSA database contains also NF membranes produced by Dow Filmtec (USA) including the NF270 and NF90. The performance of this prediction tool was then checked for the NF treatment of the studied Tunisian groundwaters. It was demonstrated previously that NF270 and NF90 should be the best choice for desalting Feed 1 and Feed 2,

Table 5:
Parameters of permeates and productivity for treatment of Feed 3 at 10 and 14 bar

	Applied pressure	Cl^- mg/L	Na^+ mg/L	Salinity mg/L	Permeate flow rate L/h m^{-2}	Recovery (%)
NF90	10	104	64	200	48	10.1
	14	58.6	41.7	135	72.2	15.2
BW30	10	57	34	99[a]	21	4.4
	14	43.7	37	77.2[a]	32.8	6.9

[a]Not complying with the Tunisian standards for drinking water.

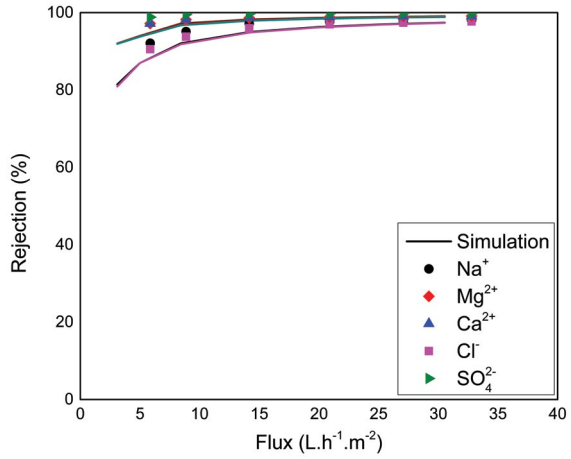

Fig. 6. Ion rejections as a function of permeate flux for Feed 3 treated with BW30. Solid curves are simulation results obtained with ROSA and symbols the experimental results.

respectively. Fig. 7 presents the modeling of ion rejections as a function of the permeate flow rate in these two cases.

It can be seen in Fig. 7 that ROSA simulation gives the right order for ion rejection experimentally found as $SO_4^{2-} \geq Mg^{2+} \geq Ca^{2+} > Na^+ > Cl^-$. However, the ROSA predictions systematically overestimate the rejection performance of the membrane representative of group 1 (NF270). This is especially seen in the case of the monovalent ions with a minimum deviation of about 40% and 25% for chloride and sodium on the high flux plateau (applied pressure 10 bar and higher). On the other hand, the simulation of divalent ion rejection appears to be much better with a difference of less than 10% in the same conditions. For purposes of comparison, the same modeling was performed with NF90 (group 2). Closer agreement between the experimental monovalent ion rejection data and the ROSA simulation curves (about 10% at plateau) were obtained in this case. Actually, group 2 NF membranes exhibit performance similar to those of BWRO membranes. Consequently, although it is thought that the transport mechanism is different between these two kinds of membranes (tight NF and RO), the ROSA software can lead to a good estimation of the NF90 performance. In contrast, this is not the case for group 1 NF membranes. With a higher selectivity between monovalent and divalent ions (a signature of NF membranes), the difference in transport mechanism is brought to the forefront and experimental data for monovalent ion rejection could not be properly predicted by the ROSA software. Another point to mention is the discrepancy between the permeate flux simulation and experimental data. As seen in Fig. 7, the maximum flux at 15 bar is about 50% and 25% lower than the values obtained with NF270 and NF90, respectively.

In order to get further insight into which factors are not properly taken into account by ROSA, additional NF

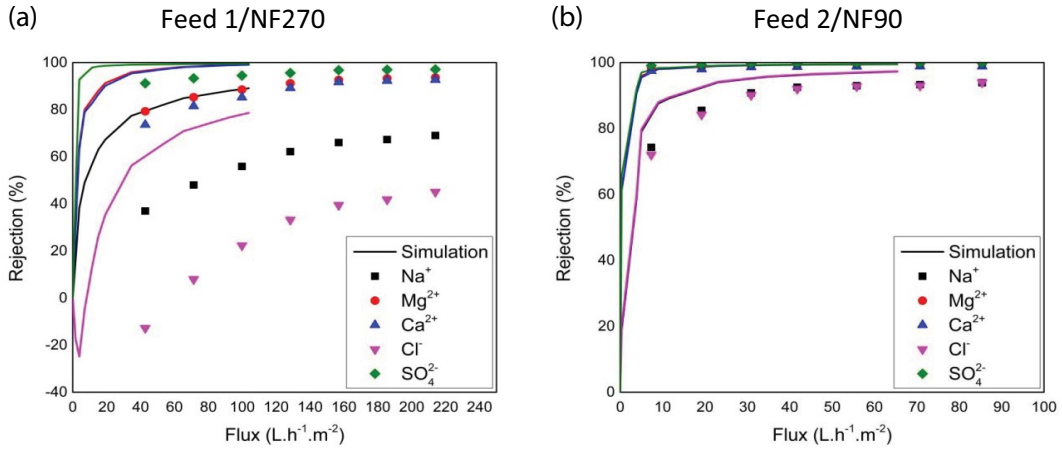

Fig. 7. Ion rejections as a function of permeate flux for Feed 3 treated with BW30. Solid curves are simulation results obtained with ROSA and symbols the experimental results.

experiments with a single monovalent salt (NaCl) were undertaken using the NF270 membrane in the range of applied pressure 3–15 bar. In a first experiment, the feed salt concentration was varied from 10^{-3} to 10^{-1} M at a fixed pH = 6 in order to examine how the feed ion content affects the ROSA prediction in the case of NF membranes. This range corresponds to chloride ion concentrations from 35.5 to 3,550 mg/L and sodium ion concentrations from 23 to 2,300 mg/L. Fig. 8 (a) presents the ROSA simulation results and the experimental data. An increase of the feed ionic strength causes a drastic decrease in the experimental ion rejection. Actually, the extent of electrical interactions is strongly limited by the charge screening occurring at high ionic strength, which accounts for a drop in monovalent rejection [39]. This effect linked to a decrease of the Debye length is well reflected in the zeta potential change of the NF270 membrane surface as a function of ionic strength and it is particularly marked for pH values higher than 6 (Fig. 9b) [40]. By contrast no change is observed in the ROSA simulations. It can, however, predict fairly well the ion rejection for low salt concentrations around 10^{-3} M. It can be concluded that the ROSA modeling does not take into account the variation of electrical interactions with changing feed composition. This could explain why the ROSA prediction tool cannot predict the rejection behavior of NF membranes given that interfacial Donnan (electrostatic) exclusion is one of the predominant mechanisms governing ion rejection in this case.

The increase in ionic strength leads also to a decline of the experimental permeate flow rate particularly noticeable in the concentration range between 10^{-2} and 10^{-1} M. This observation is due to the rise in osmotic pressure (Fig. 8a). Although this qualitative effect on membrane performance is well taken into account by the ROSA modeling, the predicted amplitude of the flow rate drop is much greater than the experimentally observed one. Apart from the large overestimation of ion rejection seen in Fig. 8a in the case of 10^{-1} M NaCl feed, the pure water permeability data input in the ROSA database (about 11 L/h m^2 bar) that is one and half times lower than the experimental one (16.3 ± 1.0 L/h m^2 bar)

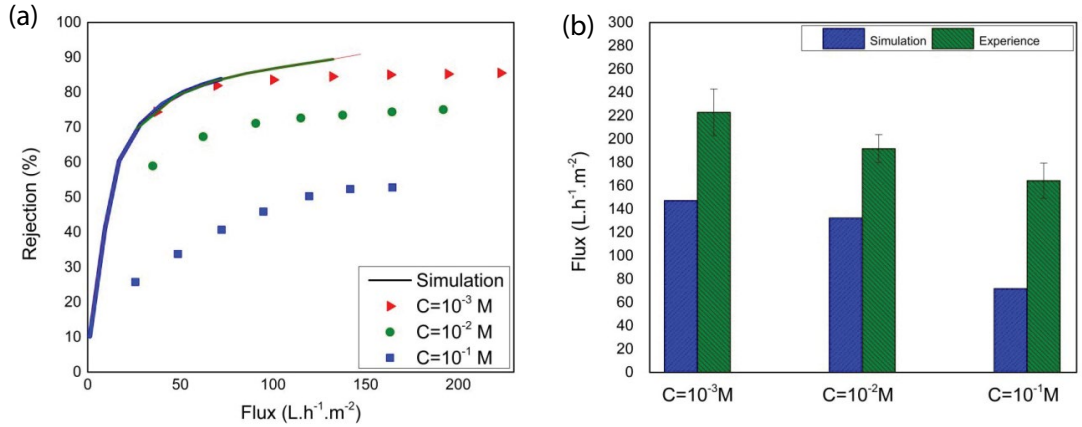

Fig. 8. Comparison between simulated and experimental ion rejections as a function of permeate flux for different NaCl feed concentration at pH 6 (a) and the corresponding permeate flux as a function of NaCl feed concentration (b). Solid curves are simulation results obtained with ROSA and symbols the experimental results.

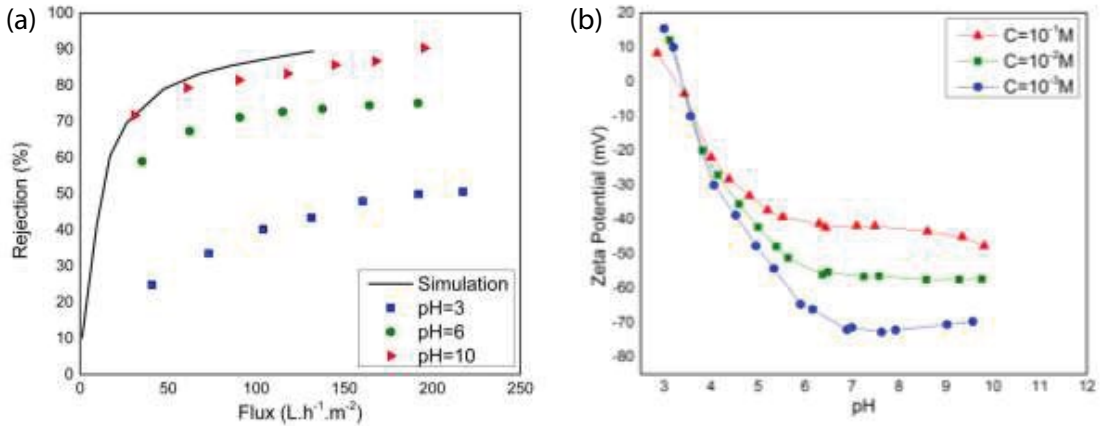

Fig. 9. Ion rejections as a function of permeate flux for 10^{-2} M NaCl feed at various pH (a). Solid curves are simulation obtained with ROSA and dots the experimental results. Zeta potential of the NF270 membrane surface as a function of pH and KCl concentration (b).

could likely be responsible of the observed discrepancy for the 10^{-3} and 10^{-2} M NaCl feeds.

The membrane surface charge originates from the ionization of functional groups and/or the adsorption of charged species, especially in the case of polyvalent ions [41]. As seen in Fig. 9b, membrane surface charge is strongly affected by pH of the contacting solution (isoelectric point between 3 and 4) [42]. NF270 becomes more negatively charged as the pH increases before reaching a plateau at neutral pH. Next, a second experiment was designed to examine if this effect is taken into account by ROSA. Fig. 9a displays the NF270 ion rejection for a 10^{-2} M NaCl feed at three different pH values (3, 6 and 10). This concentration was chosen to discriminate the effect of pH change from that of ionic strength. It appears from the experimental data that the rejection at 15 bar decreases from about 90% to 50% when decreasing the pH from 10 to 3. This result is consistent with the membrane charge inferred from the zeta potential values shown in Fig. 9b. A higher membrane charge is expected to lead to a higher ion rejection in the case of a single salt due to the Donnan exclusion. Interestingly, ROSA can predict more or less the rejection at pH values corresponding to the plateau (pH = 10) but fails at lower pH when the membrane surface charge shows a large variation. We do not know how the ROSA software is designed for predicting the rejection performance of NF membranes, but it appears clearly that the electrical interactions between the charged solutes and the membrane are not considered in their full complexity and totality. To further investigate this issue, the following section is devoted to the validation of a prediction tool, Nanoflux®, specifically designed to address the particularities of NF membrane transport.

3.2.2. *Nanoflux® validation*

The Nanoflux® prediction tool is based on an internal database containing the specific membrane parameters (pore radius r_p, normalized membrane charge X_i and effective pore length l_{eff}) required to solve the set of equations describing the HET model. This database is built from the rejection data of neutral solutes (r_p) and of representative single salts including NaCl, Na_2SO_4, $MgSO_4$, $CaCl_2$ in different conditions of pH and concentration. By decomposing the feed solution in a combination of single salts, the software defines a new set of membrane parameters by mathematical interpolation according to the feed composition and pH. Calculation using the HET model then enables Nanoflux® to predict membrane performance in terms of flux and ion rejection. For instance, Table 6 gives the different membrane parameters used by Nanoflux® for establishing the simulation curves presented below.

From these data, it can be seen clearly that the feed composition impacts the normalized membrane charge and thereby the electrical interactions with the solutes. As indicated before, the membrane charge density decreases with the increase of the feed ionic strength by charge screening. This accounts for the reduction of X_i from Feed 1 to Feed 2. However, an increase of this parameter is observed for Feed 3 in spite of a further increase of the salt content. As can be noted from the composition of Feed 3 in Table 2, the pH of this solution is 8 compared with about 6 for the previous ones, explaining the increase membrane charge. Thus, by taking into account the electrical interactions more specifically, prediction of NF membrane performance can be more accurate.

For example, Figs. 10 and 11 present the comparison between the simulation curves given by Nanoflux® for the

Table 6
Parameters determined by Nanoflux® for the modeling performance of the studied NF membranes as a function of the used feed solutions

	NF270			NF90		
	r_p (nm)	X_i	l_{eff} (μm)	r_p (nm)	X_i	l_{eff} (μm)
Feed 1	0.525	–1.245	3.167	0.42	–46.63	8.92
Feed 2	0.525	–0.748	13.84	0.42	–22.45	21.0
Feed 3	–	–	–	0.42	–30.00	35.0

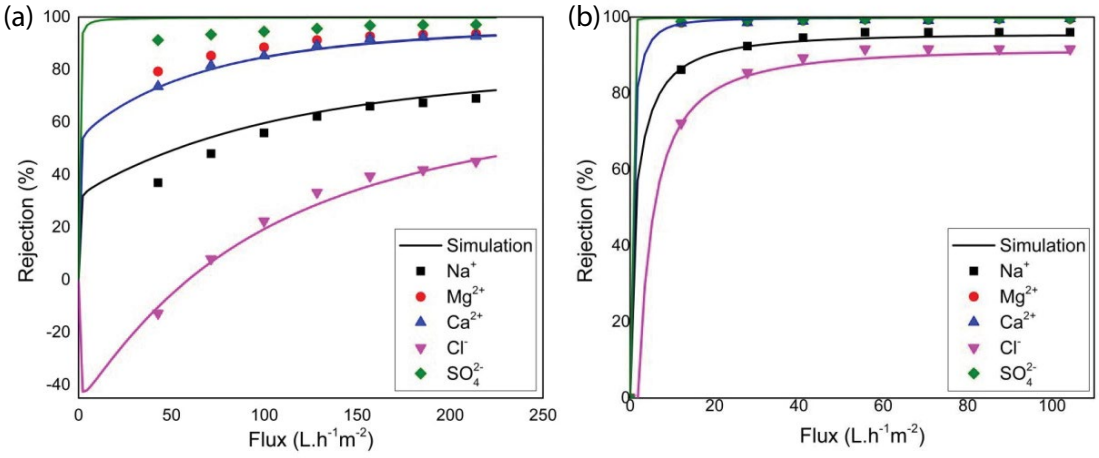

Fig. 10. Ion rejections as a function of permeate flux for Feed 1 nanofiltered by NF270 (a) and by NF90 (b). Solid curves are simulation results obtained with Nanoflux® and symbols the experimental results.

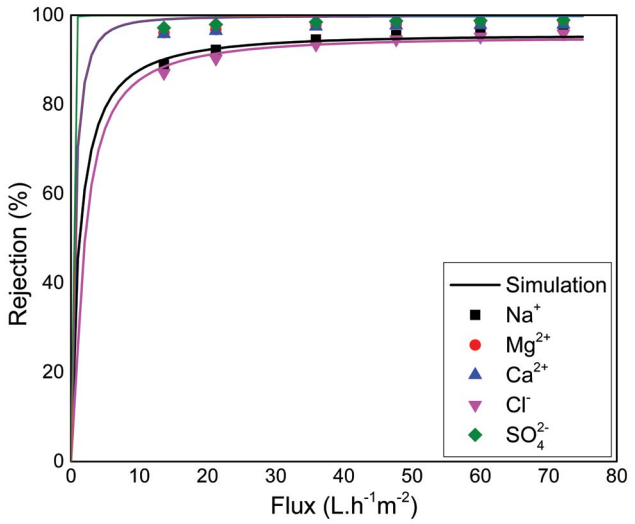

Fig. 11. Ion rejections as a function of permeate flux for Feed 3 nanofiltered by NF90. Solid curves are simulation results obtained with Nanoflux® and symbols the experimental results.

ion rejection in the case of Feed 1 using NF270 and NF90 and those for Feed 3 using NF90, respectively. As can be seen, the experimental rejections of the five ions (Na^+, Cl^-, SO_4^{2-}, Ca^{2+} and Mg^{2+}) are well fitted by the modeling enabling a reliable assessment of membrane performance in all cases studied.

4. Conclusion

It was demonstrated in this study that the two predominant brackish water types found in South Tunisia can be treated by NF technology. Two groups of NF membranes were considered depending on their divalent/monovalent selectivity. The advantage of this approach is that a better productivity of permeates complying with the Tunisian requirements for drinking water can be obtained. The conclusion of this study can be summarized in the following way:

- The sulfate/chloride ratio appeared to be the key factor for choosing the more appropriate membrane to treat specified low salinity groundwaters. Thus, it was found that Tunisian groundwaters can be roughly divided into two families separated by the sulfate/chloride ratio of about 1. The experimental results showed that the group 1 NF membranes as exemplified by NF270 are suitable for treatment of low salinity feeds having a large proportion of sulfate ions over chloride ions. By contrast, the group 2 NF membranes with ion rejections close to those of RO (similar to NF90) provided an optimal compromise for groundwaters from the sedimentary coastal aquifers containing a high proportion of chloride ions.
- Validation of available software was undertaken to have a decision-making tool for selecting the right membrane as a function of the feed to be treated and the water quality to be produced. It was shown that Nanoflux®, a prediction tool specifically designed for taking into account the complexity of NF membrane transport, can be a useful tool for this technology. On the other hand, the ROSA software designed for RO was not found to be generally useful for the prediction of NF membrane performance because it does not appear to account for the electric interactions between membrane and solutes.

Symbols

A	—	Membrane area, m^2
C_i^f	—	Concentration of ion i in the feed, M
C_i^p	—	Concentration of the ion i in the permeate, M
C_{tot}	—	Total salt concentration, M
$\bar{c}_i$	—	Concentration of ion i inside the membrane, M
D_i	—	Effective diffusion coefficient of ion i in the membrane, m^2/s
F	—	Faraday constant, C mol^{-1}
J_i	—	Molar flux density of ion i, 1/mol m^2 s
J_v	—	Volume flux density based on the membrane area, m/s or L/h m^2
J_c	—	Electric current density, C/m^2 s
$K_{i,d}$	—	Hindrance factor for diffusion
$K_{i,c}$	—	Hindrance factor for convection
L_p^0	—	Pure water permeability, L/h bar m^2
l_{eff}	—	Effective active NF membrane layer thickness, μm
lm	—	Active NF membrane layer thickness, μm
P	—	Average fluid pressure, bar
r_p	—	Pore radius, nm
R	—	Gas constant, J mol^{-1} K^{-1}
R_i	—	Ion rejection of ion i
T	—	Absolute temperature, K
V_p	—	Volume of permeate, L
X_m	—	Effective membrane charge, $moles/m^3$
X_i	—	Normalized membrane charge
z_i	—	Valence of ion i
Δt	—	Time, h
$\Delta\phi_D$	—	Donnan potential, mV
ϕ	—	Electric potential, mV
Φ_i	—	Steric partitioning coefficient of ion i local ion charge density
σ	—	Surface charge density, C/m^2
ρ	—	Ion charge intensity, C/m^3

References

[1] M. Elloumi, La gouvernance des eaux souterraines en Tunisie, "Groundwater governance in the Arab World –Taking Stok and addressing the challenges", IMWI publication, 2016.
[2] ITES, Etude stratégique: Système hydraulique de la Tunisie à l'horizon 2030, 2014, p. 222.
[3] A. Hamdane, La gestion des ressources en eau souterraines (nappes et aquifères) comme biens communs: Cas de la Tunisie, Synthèse régionale sur l'approche économique de la gestion de la demande en eau en Méditerranée, 2014.
[4] M.F. Ben Hammouda, P. Carreira, J.M. Marques, H. Egenkamps, Geochimical and isotopic investigation to study the origin of mineralization of the coastal aquifer of Sousse, Tunisia, Procedia Earth Planet Sci., 7 (2013) 61–64.
[5] NT.09.14 Normes Tunisiennes – Eaux destinées à la consommation humaine à l'exclusion des eaux conditionnées, 2013.
[6] V.G. Gude, Desalination of deep groundwater aquifers for freshwater supplies – challenges and strategies, Groundwater Sustain. Dev., 6 (2018) 87–92.

[7] S.S. Shenvi, A.M. Isloor, A.F. Ismail, A Review on RO membrane technology: developments and challenges, Desalination, 368 (2015) 10–26.
[8] A.J. Karabelas, D.C. Sioutopoulos, New insights into organic gel fouling of reverse osmosis desalination membranes, Desalination, 368 (2015) 114–126.
[9] Q. She, R. Wang, A.G. Fane, C.Y. Tang, Membrane fouling in osmotically driven membrane processes: a review, J. Membr. Sci., 499 (2016) 201–233.
[10] M. Badruzzaman, A. Subramani, J. DeCarolis, W. Pearce, J.G. Jacangelo, Impacts of silica on the sustainable productivity of reverse osmosis membranes treating low salinity brackish groundwater, Desalination, 279 (2011) 210–218.
[11] A.W. Mohammad, Y.H. Teow, W.L. Ang, Y.T. Chung, D.L. Oatley-Radcliffe, N. Hilal, Nanofiltration membranes review: Recent advances and future prospects, Desalination, 356 (2015) 226–254.
[12] M. Talaeipour, J. Nouri, A.H. Hassani, A.H. Mahvi, An investigation of desalination by nanofiltration, reverse osmosis and integrated (hybrid NF/RO) membranes employed in brackish water treatment, J. Environ. Health Sci. Eng., 15 N° 1 (2017) 15–18.
[13] N. Yousefi, A. Fatehizedeh, K. Ghadiri, N. Mirzaei, S.D. Ashrafi, A.H. Mahvi, Application of nanofilter in removal of phosphate, fluoride and nitrite from groundwater, Desal. Wat. Treat., 57 (2016) 11782–11788.
[14] A.H. Mahvi, M. Malakootian, A. Fatehizadeh, M.H. Ehrampoush, Nitrate removal from aqueous solutions by nanofiltration, Desal. Wat. Treat., 29 (2011) 326–330.
[15] B. Van der Bruggen, Nanofiltration in Encyclopedia of Membrane Science and Technology, E.M.V. Hoek, V.V. Tarabara, Eds., John Wiley & Sons, Inc, 2013.
[16] https://dowac.custhelp.com/app/answers/detail/a_id/4925/~/filmtec-membranes---nanofiltration---mwco, (17 Juin 2019)
[17] http://synderfiltration.com/nanofiltration/membranes/, (17 Juin 2019)
[18] https://trisep-membranes.squarespace.com/s/TS40.pdf, (17 Juin 2019)
[19] K. Kősutić, D. Dolar, B. Kunst, On experimental parameters characterizing the reverse osmosis and nanofiltration membranes' active layer, J. Membr. Sci., 282 (2006) 109–114.
[20] https://trisep-membranes.squarespace.com/s/TS80.pdf, (17 Juin 2019)
[21] http://membranes.com/solutions/products/nf/esna-2/, (17 Juin 2019)
[22] Y. Song, T. Li, J. Zhou, Z. Li, C. Gao, Analysis of nanofiltration membrane performance during softening process of simulated brackish groundwater, Desalination, 399 (2016) 159–164.
[23] X. Su, Y. Song, T. Li, G Congjie, Effect of feed water characteristics on nanofiltration separating performance for brackish water treatment in the Huanghuai region of China, J. Water Process Eng., 19 (2017) 147–155.
[24] Y. Song, J. Xu, Y. Xu, X. Gao, C. Gao, Performance of UF–NF integrated membrane process for seawater softening, Desalination, 276 (2011) 109–116.
[25] L.D. Nguyen, S. Gassara, M.Q. Bui, F. Zaviska, P. Sistat, A. Deratani, Desalination and removal of pesticides from surface water in Mekong Delta by coupling electrodialysis and nanofiltration, Environ. Sci. Pollut. Res. Int., (2018). doi. org/10.1007/s11356-018-3918-6.
[26] H. Chmiel, X. Lefebvre, V. Mavrov, M. Noronha, J. Palmeri, Computer Simulation of Nanofiltration, Membranes and Processes, In: M. Rieth, W. Schommers, Eds., Handbook of Theoretical and Computational Nanotechnology, American Scientific Publishers, Vol. 5, 2006, pp. 93–214.
[27] A. Altaee, A Computational Model to Estimate the Performance of 8 inches RO Membranes in Pressure Vessel, J. Membr. Sep. Technol., 1 (2012) 60–71.
[28] X.L. Wang, T. Tsuru, M. Togoh, S. Nakao, S. Kimura, Transport of organic electrolytes with electrostatic and steric-hindrance effects through nanofiltration membranes, J. Chem. Eng. Jpn., 28 (1995) 372–380.
[29] W.R. Bowen, H. Mukthar, Characterization and prediction of separation performance of nanofiltration membranes, J. Membr. Sci., 112 (1996) 263–274.
[30] X. Lefebvre, J. Palmeri, P. David, Nanofiltration theory: an analytic approach for single salts, J. Phys. Chem. B, 108 (2004) 16811–16824.
[31] J. Palmeri, J. Sandeaux, R. Sandeaux,, P. David, C. Guizard, P. Amblard, J.F. Diaz, B. Lamaze, Modeling of multi-electrolyte transport in charged ceramic and organic nanofilters using the computer simulation program NanoFlux, Desalination, 147 (2002) 231–236.
[32] X. Lefebvre, J. Palmeri, J. Sandeaux, R. Sandeaux, P. David, B. Maleyre, C. Guizard, P. Amblard, J.F. Diaz, B. Lamaze, Nanofiltration modeling: a comparative study of the salt filtration performance of a charged ceramic membrane and an organic nanofilter using the computer simulation program nanoflux, Sep. Purif. Technol., 32 (2003) 117–126.
[33] J. Palmeri, N. Ben Amar, H. Saidani, A. Deratani, Process modeling of brackish and seawater nanofiltration, Desal. Wat. Treat., 9 (2009) 26–271.
[34] X. Lefebvre, J. Palmeri, Nanofiltration Theory: Good co-ion exclusion approximation for single salts, J. Phys. Chem. B, 109 (2005) 5525–5540.
[35] H. Bukšek, T. Luxbacher, I. Petrinić, Zeta potential determination of polymeric materials using two differently designed measuring cells of an electrokinetic analyzer, Acta Chim. Slov., 57 (2010) 700–706.
[36] S. Gassara, W. Chinpa, D. Quemener, R. Ben Amar, A. Deratani, Pore size tailoring of poly(ether imide) membrane from UF to NF range by chemical post-treatment using aminated oligomers, J. Membr. Sci., 436 (2013) 36–46.
[37] M. Pontié, H. Dach, J. Leparc, M. Hafsi, A. Lhassani, Novel approach combining physico-chemical characterizations and mass transfer modelling of nanofiltration and low pressure reverse osmosis membranes for brackish water desalination intensification, Desalination, 221 (2008) 174–191.
[38] A. Azaïs, J. Mendret, S. Gassara, E. Petit, A. Deratani, S. Brosillon, Nanofiltration for wastewater reuse: counteractive effects of fouling and matrice on the rejection of pharmaceutical active compounds, Sep. Purif. Technol., 133 (2014) 313–327.
[39] J. Luo, Y. Wan, Effects of pH and salt on nanofiltration—a critical review, J. Membr. Sci., 438 (2013) 18–28.
[40] L. Thomas, C. Bryan, T. Cath, Does the surface zeta potential approach zero at high salinity?, Advances in Civil, Environmental, and Materials Research (ACEM14), Busan, Korea, 2014, pp. 24–28. http://www.i-asem.org/publication_conf/acem14/3.MWT/T3C.3.MW251_386F.pdf
[41] W.B.S. de Lint, N.E. Benes, J. Lyklema, H.J.M. Bouwmeester, A.J. van der Linde, M. Wessling, Ion adsorption parameters determined from zeta potential and titration data for a y-alumina nanofiltration membrane, Langmuir, 19 (2003) 5861–5868.
[42] P. Ortiz-Albo, R. Ibañez, A. Urtiaga, I. Ortiz, Phenomenological prediction of desalination brines nanofiltration through the indirect determination of zeta potential, Sep. Purif. Technol., 210 (2019) 746–753.

Supplementary information

Design parameters for ROSA
Fixed parameters:

well water SDI < 3,
T = 25°C,
feed rate = 0.47 m^3/h,
one filtration module: type 2450,
factor flow = 0.85,
pump efficiency = 0.8,

Example of filtration Fig. 7b:

Feed Flow to Stage 1	0.47	m^3/h
Raw Water Flow to System	0.47	m^3/h
Feed Pressure	4	bar
Flow Factor	0.85	
Chem. Dose (100% H2SO4)	0	mg/l
Total Active Area	2.6	M^2
Water Classification: Well Water SDI < 3		
Pass 1 Permeate Flow	0.03	m^3/h
Pass 1 Recovery	6.54	%
FeedTemperature	25	C
Feed TDS	3362.2	mg/l
Number of Elements	1	
AveragePass 1 Flux	11.81	lmh
Osmotic Pressure:		
Feed	2.08	bar
Concentrate	2.2	bar
Average	2.14	bar
Average NDP	1.65	bar
Power	0.07	kW
SpecificEnergy	2.13	kWh/m^3

Results :

Name	Feed (mg/L)	Adjusted Feed	Concentrate	Permeate		
			Stage 1	Stage 1	Total	Rejection
Na	837	862.64	916	99.75	99.75	89.1
Mg	98.56	98.56	105.32	1.95	1.95	98.15
Ca	208	208	222.26	4.06	4.06	98.17
Cl	1400	1400	1486.94	157.05	157.05	89.44
SO4	793	793	847.55	13.05	13.05	98.46
TDS	3336.56	3362.2	3578.07	275.86	275.86	92.29
pH	6	6	6	6	6	